



Variation in Structural, Electrical and Optical Properties of Selenium Nanowires After Irradiation with Ni⁶⁺ Ions

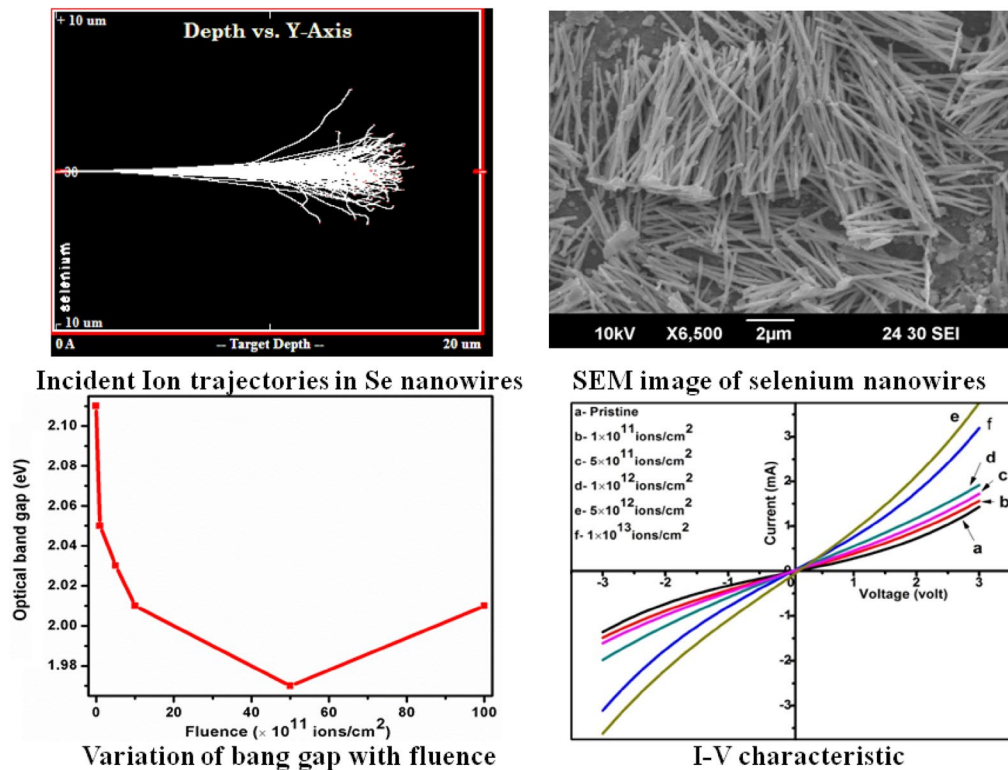
Suresh Panchal¹ · R. P. Chauhan¹

Received: 10 September 2018 / Accepted: 20 November 2018 / Published online: 7 December 2018
© The Korean Institute of Metals and Materials 2018

Abstract

The effect of Ni ion irradiation on selenium nanowires of 80 nm diameter is studied in the present work. Se nanowires were prepared by using electrodeposition technique in polycarbonate membrane. Changes in the structural, optical and electrical properties are studied using XRD, UV/Vis spectroscopy and current–voltage characteristics, of the pristine and irradiated samples. X-ray diffraction study confirms the variation in peak intensity without any shifting in peak position. Variation in texture coefficient and grain size was clearly observed which is a consequence of changing plane orientation, irradiation induced grain growth and grain fragmentation. A decrease in the optical band gap takes place due to interstitial energy band states in the vicinity of conduction and valence band. IVC also shows variation in the conductivity which is due to the generation of current carriers with the passage of energetic ions.

Graphical Abstract



Extended author information available on the last page of the article

Keywords Ion irradiation · Selenium nanowires · Structural analysis · Optical analysis · Electrical properties · Impedance

1 Introduction

There is considerable interest in investigating the properties of II–VI group semiconducting nanomaterials due to their wide application. Nanowires are the smallest building blocks towards next-generation technology and are broadly implemented in the formation of nanodevices. During the last few years, many researchers have stated various one-dimensional based nanodevices like solar cells, field effect transistors (FETs), nanogenerators etc. [1–4].

Selenium is a p-type semiconductor having energy band gap of the order of 1.6 eV, belonging to VI group. One dimensional selenium nanowires are studied extensively due to their high catalytic activity, improved photoconductivity and better electrical conduction [5, 6]. Selenium nanowires have immense utility in batteries, solar cells, xerography and light measuring devices. 1D selenium nanostructures may act as a major element for photoconductor due to their spectral response in the entire visible range. Different researchers used different methods for the synthesis of selenium nanowires, Liao et al. [7] synthesize ultra long selenium nanowires and bundles via CTAB assisted solvothermal method. Kumar et al. [8] used template-assisted electrodeposition to obtain vertically aligned selenium nanowires of uniform diameter. Steichen et al. [9] synthesize trigonal selenium nanorods by electrodeposition technique at high temperature from ionic liquid. Chen et al. [10] used a facile template-free solution method to prepare trigonal selenium nanowires on large scale. There are so many techniques for the synthesis of 1D nanostructures like vapor segment growth, sonochemical approach, self-seeding system template-based approach, hydrothermal method, laser ablation, biomolecule-assisted synthesis, template free, solution phase approach etc. Among these entire techniques, template-assisted electrodeposition provides a simple, economical and skillful technique with the help of which we are able to get uniform growth of free standing nanowires with controlled shape, diameter and length at large scale [11].

Energetic ion beams have been distressed by researchers in divergent ways in the field of materials science. Ion irradiation is studied extensively as a unique tool to modify the properties of materials at different length scales in a controlled way. The structural, electrical and optical properties of semiconductor nanostructures can be easily modified by irradiation or implantation process. Energetic ions penetrating a solid lose energy via two processes (1) elastic collision, in which direct transfer of energy to the target material takes place, also called nuclear energy loss (S_n) and (2) inelastic collision i.e. electronic excitation and ionization of target atoms, also known as electronic energy loss (S_e). The later

process is prevalent in action of swift heavy ion (SHI) irradiation. On its passage in the material, energetic ion leads to the excitation and ionization process which results in the different kind of defects like; disorder clusters, vacancies and, dislocations which have an effect on the energy levels and modifications in the physical properties of the materials in a controlled way [12–17]. The formation of defects in any material depends on the energy of the incident ion and its weight. The presence and distribution of these defects greatly affect the performance of many devices like sensors, Schottky diodes, solar cells etc. Moreover trapping and recombination of charge carriers are mainly accountable for the modification in optical and electrical properties of the material [18, 19]. Significant modification in the electric and optical properties was observed in CdSe thin films under swift heavy ion irradiation [20]. An appreciable change in the optical properties of graphene nanosheets was observed on low energy nitrogen ion implantation [21]. Impact of energetic ions on nanomaterials plays an important role in tailoring the properties of nanomaterials like crystallinity, free charge density, conductivity etc. Recent studies also show that irradiation have fruitful effects on nanomaterial properties. Swift heavy ions have a potential to modify the nanomaterial properties by huge energy transferred through electronic excitation process. Changes in the electrical and optical properties of Se nanowires due to the formation of defects require a detailed investigation. Change in the properties of nanomaterial on irradiation is reported in our previous studies [22–25]. But the effects of irradiation on the selenium nanowires, are not explored much.

In the present investigation, we have examined the effect of 80 MeV Ni^{6+} ions irradiation on Se nanowires (80 nm) for different fluences ranging from 1×10^{11} to 1×10^{13} ions/cm². The energy of the nickel ions is so chosen, that they may easily cross the whole length of nanowires (10 μ m).

2 Experimental Details

2.1 Synthesis

AR grade chemicals, purchased from Sigma Aldrich Company, were used for synthesis of selenium nanowires. A three-electrode setup was used for the electrodeposition of selenium nanowires. Electrolyte consists of selenium dioxide (SeO_2) and boric acid (H_2BO_3) and pH of the solution was maintained around 2. Polycarbonate membrane, which had pore of 80 nm diameter, was used for deposition. One side of the membrane was coated with gold–palladium alloy and was then placed on copper tape and deposition was thereafter performed in a cell

made of Perspex, for 7 min at room temperature (32 ± 2) °C. Deposition reaction was governed by the use of potentiostat (SP-240 Biologic) via chrono-amperometry process in which all the potentials were applied with respect to the reference electrode (Ag/AgCl). The copper tape, along with polycarbonate membrane, works as a working electrode and for counter electrode, a thin wire of platinum was used whose diameter was around 5 mm. During electrochemical reaction filling of the pores takes place and after complete deposition, the sample was collected carefully and placed in desiccator.

2.2 Irradiation Parameters

The nanowires were irradiated with 80 MeV Ni⁶⁺ ions beam using 15UD pelletron facility available at Inter University Accelerator Centre (IUAC), New Delhi, India, for different fluence ranging from 1×10^{11} to 1×10^{13} ions/cm². The samples were mounted on a metal ladder which enables the direct exposure of nanowires to ion beam in a vacuum chamber having the pressure of 6×10^{-6} torr. All irradiation processes were carried out at this high vacuum. The beam was magnetically scanned over an area of 1×1 cm² area. To avoid heating effect the beam current was maintained at 1 pA [1 pA (particle nanoampere) = 6.25×10^8 particles/cm²/s].

2.3 SRIM TRIM Simulation

To understand the energy loss mechanism and range of the projectile, SRIM TRIM simulation were performed. Simulation parameters for the 80 MeV Ni ion irradiation parameters like stopping powers (S_e and S_n), projected range and ion straggling are tabulated in Table 1.

SRIM comprises of comprehensive Monte Carlo software known as transport of ions in matter (TRIM), which provide an in depth study of ion damage cascades and the distribution of ions inside the material under consideration. SRIM/TRIM simulation supplies a quantitative estimation of the irradiation-induced damages within the target material. In addition to longitudinal damages, energetic ions may also produce lateral damages into the host material along their trajectories. These defects are in the form of interstitial spaces, electronic excitations, vacancies, and amorphization. TRIM simulation for 80 MeV Nickel ion beam interaction with Se NWs is as shown in Fig. 1a–d.

The anticipated ion trajectories for 3000 ions within the material are simulated in Fig. 1a. The nanowires are

uniformly affected by the irradiation as the range of nickel ion was found to be 15.07 μm which is much larger than the length of the nanowires (10 μm) and therefore ions probability of implantation is negligible. The values of electronic (S_e) and nuclear (S_n) energy losses are 9.148×10^2 eV/Å and 2.357 eV/Å, respectively. Therefore the major part of the Ni⁶⁺ ion energy is imparted to the target material through electronic energy loss. Some limitations are also there with TRIM simulation as it makes computation only for a smooth surface and does not make any consideration for the impacts and damage produced by past embedded particles. As indicated by TRIM-simulation, every Ni ion of this energy can produce 24,998 displacements including 24,998 vacancies and 0 replacement collision before stopping. Here ionization is the process of transfer of projectile energy to the target electron and recoil refers to the energy transferred from the recoil selenium atoms to the electrons. From the simulation, it can be accomplished that the energetic Ni⁶⁺ ions lead to the creation of lattice defects in the form of vacancies and displacements on their passage through the selenium nanowires.

2.4 Characterization

X-ray of 1.54 Å wavelength was used for the structural analysis, which was taken from the Rigaku Miniflex II table top machine. Evaluation of crystal size was made from peak broadening by Scherrer method. JEOL JSM-6390 LV SEM was used for morphological analysis, which was taken at 15 kV after the removal of polycarbonate membrane. Before SEM Analysis sample surface was made conducting, for which sample was coated with gold–palladium alloy using JEOL JFC-1600 Auto Fine coater Unit. UV-spectroscopy is an important tool which provides information about band gap. Optical properties of selenium nanowires were studied via absorption spectra using a double beam UV–visible spectrometer.

3 Results and Discussion

3.1 Morphological Study

For morphological studies, SEM analysis was performed after dissolving the template. The SEM pictures not just gave information about the surface morphology of nanowires yet, in addition, portrayed the geometry of the pores of the template.

A good surface coverage with deposited NWs of 80 nm diameter was observed in the sample. Figure 2a shows the SEM image of prepared Se nanowires which confirms the uniform growth of NWs. The length of nanowires also seems to be about 10 μm. Breaking and distortion of the wires

Table 1 The energy loss and range of 80 MeV Ni⁶⁺ ions in Se NWs

Ion	Energy	Ion range	Electronic energy loss (S_e)	Nuclear energy loss (S_n)
Ni ⁶⁺	80 MeV	15.07 μm	9.148×10^2 eV/Å	2.357 eV/Å

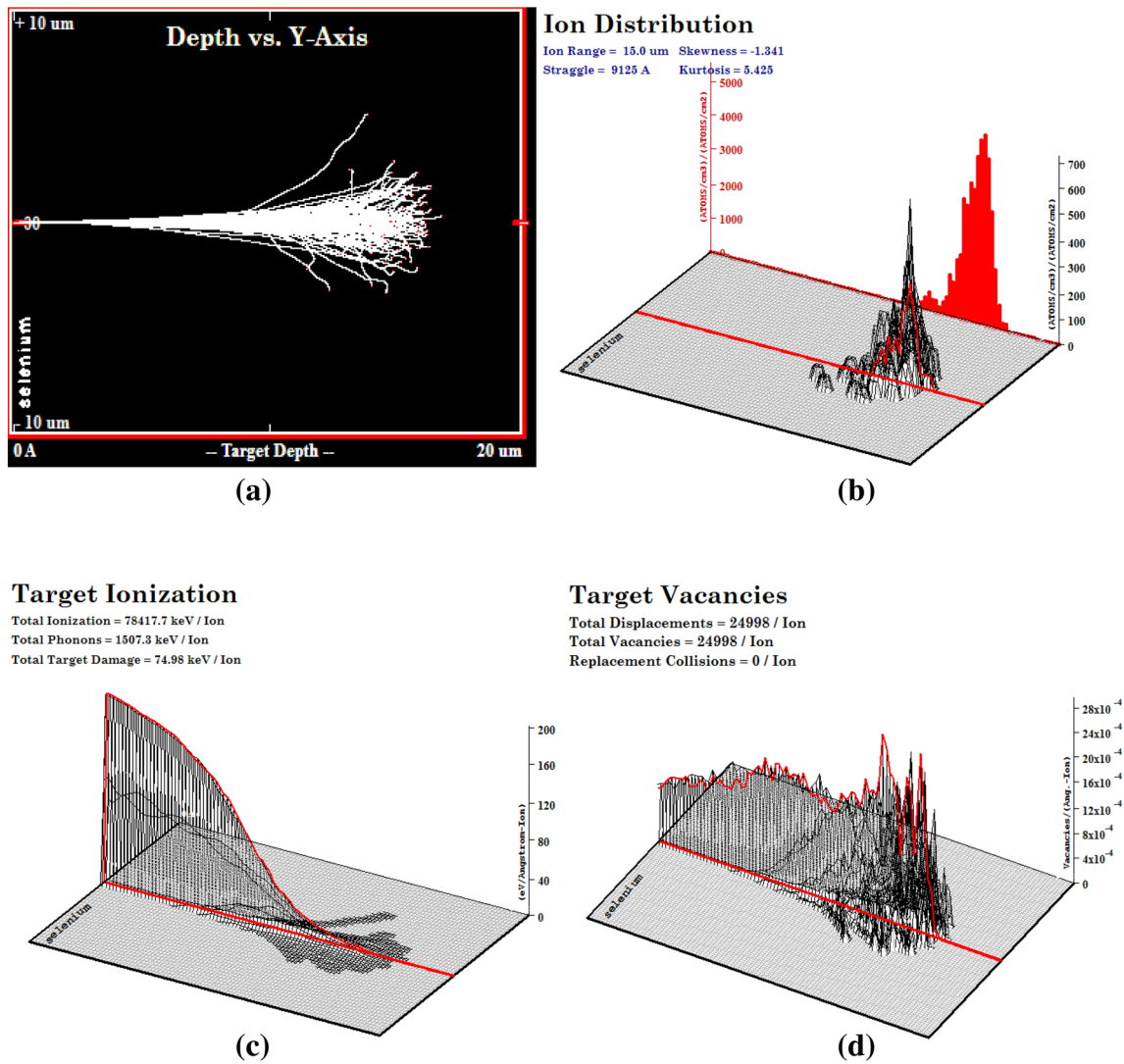


Fig. 1 a Incident Ion trajectories in Se nanowires; b ion distribution; c distribution of ionization losses; d distribution of vacancies

during the dissolution of the template is a common thing which is also clearly visible in the picture. SEM images (figures (b), (c)) of irradiated nanowires show that irradiation has no much effect on the morphology of nanowires.

3.2 Structural Analysis

To study the structural variation on irradiation, XRD spectrum was taken, as shown in Fig. 3, for different nanowires samples both pristine and irradiated. The XRD pattern closely matches with JCPDS card no. 240714, which confirms the monoclinic structure of prepared NWs. The presence of a number of peaks of the different family of planes also confirms the polycrystalline nature of pre and post-irradiated samples. The Polycrystalline material comprises of a vast number of grains each of which has its own shape and directions in space. Right through the assembling process,

grains might have a certain favored orientation with totally arbitrary (unpredictable) orientation of the lattice planes. During a few instances, polycrystalline material might also have some desired crystallographic orientation and texture [26]. Figure 3 clearly demonstrates no considerable change in the peak position, but the variation in peak intensity is clearly visible. The intensity of XRD peak is given by

$$I = F^2 p \left(\frac{1 + \cos^2 2\theta}{\sin^2 \theta \cos \theta} \right) e^{-2M} \tag{1}$$

I here refer to the relative intensity, F is the structure factor for the (hkl) plane and p is the multiplicity factor. The other factors are the Lorentz-polarization factor $((1 + \cos^2 \theta) / (\sin^2 \theta \cos \theta))$ and the temperature factor (e^{-2M}) .

The process of X-ray absorption by an atom occurs if the X-ray has either an energy exactly equal to the energy

Fig. 2 SEM image of selenium nanowires of 80 nm diameter **a** pristine, **b** after irradiation at 1×10^{11} ions/cm², **c** after irradiation at 1×10^{13} ions/cm²

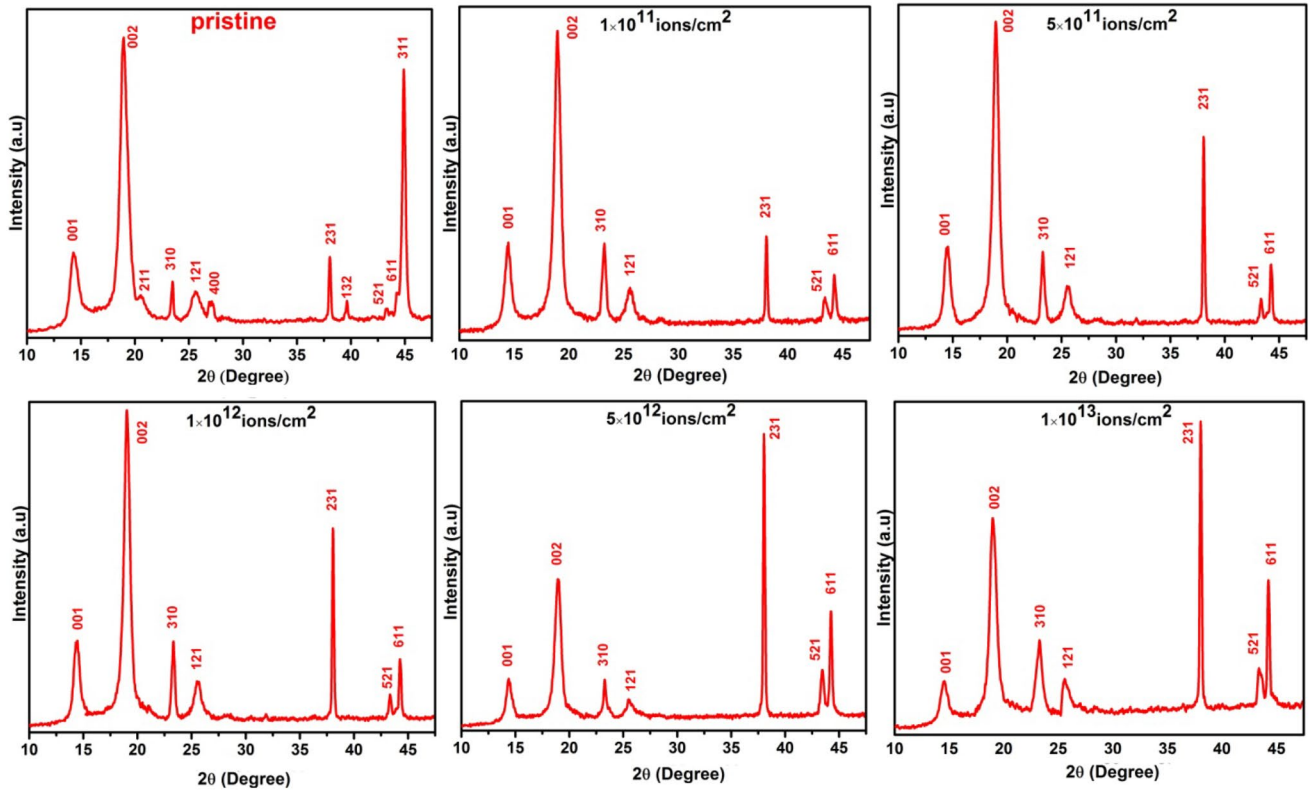
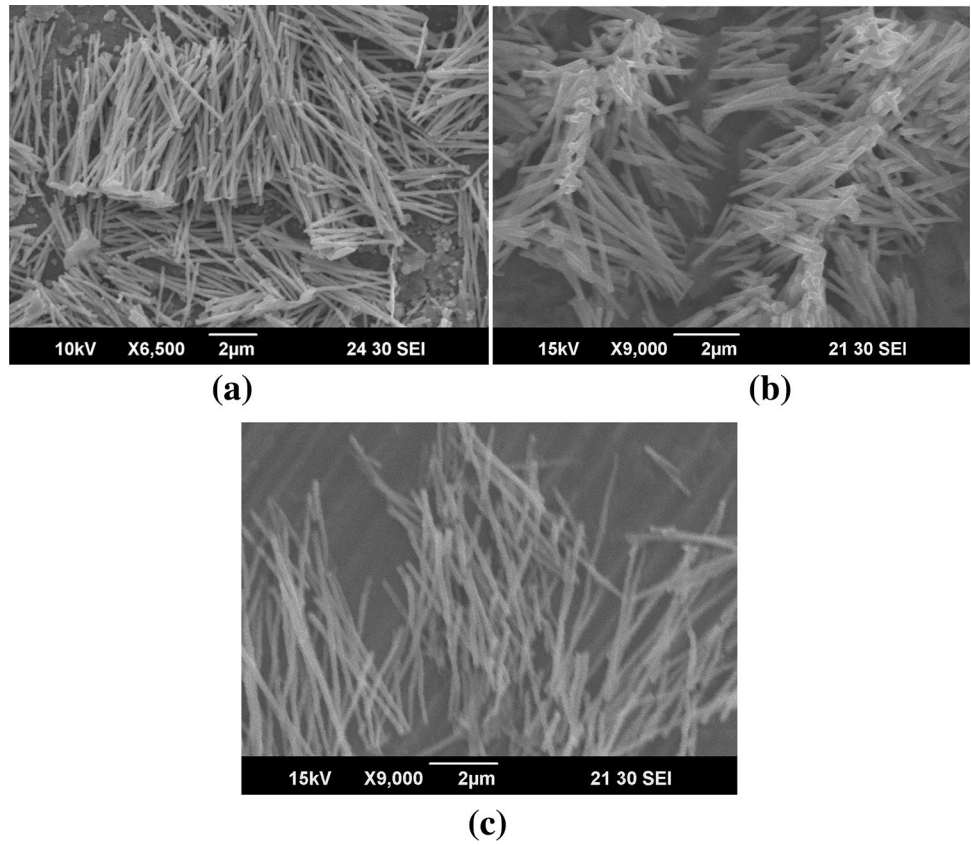


Fig. 3 XRD spectra for pristine and irradiated nanowires

difference between an energy level occupied by an atomic electron and a vacant upper energy level, or an energy sufficient to eject the atomic electron (ionization), which leads to the absorption of the initial X-ray photon and the ejection of an electron. Absorption factor is calculated from the relation K/μ where K is constant and μ is linear absorption coefficient of the sample. The absorption factor is independent of the Bragg's angle and does not affect the relative intensity of different peaks. Structure factor (F) likewise does not influence the peak intensity because of the same material. Lorentz-polarization factor also does not produce any variation in the intensity of diffraction peaks, because peak position (2θ) of pristine and irradiated samples is same. So multiplicity factor and temperature might be the conceivable reason for the variation in peak intensity. Multiplicity factor suggests the number of planes contributing toward particular diffraction peak. It incorporates all of the planes having identical interplanar spacing, an example for (110) p is twelve, and for (111) it is eight, which indicates the miller planes having equal spacing. Atoms in the lattice are continuously vibrating about their equilibrium position. As the temperature increases, this vibration amplitude will increase. One impact of this vibration is that the lattice spacing continuously changes in order that the intensity of the diffraction line decreases with increasing temperature. At the same time, background scattering increases. For a given temperature, the effect is prominent at higher Bragg angles because the d -spacing is smaller [24]. Out of remaining two factors, temperature and multiplicity factor, the temperature factor will not play a bigger role in the present case because all the samples were prepared at almost the same temperature. Therefore, only multiplication is a factor on which the peak intensity will directly depend, which can be calculated in the form of preferred orientation [27]. Preferred orientation can be evaluated on the basis of Texture Coefficient (TC) using the following equation [28, 29].

$$TC = \frac{I(hkl)}{I_0(hkl)} \bigg/ \frac{1}{n} \sum \frac{I(hkl)}{I_0(hkl)} \quad (2)$$

Table 2 Texture coefficient for pristine and irradiated NWs

Planes	Pristine	1×10^{11} ions/ cm^2	5×10^{11} ions/ cm^2	1×10^{12} ions/ cm^2	5×10^{12} ions/ cm^2	1×10^{13} ions/ cm^2
001	3.83	3.20	3.30	3.91	1.70	1.68
002	1.01	0.75	0.74	0.88	0.38	0.52
310	0.04	0.06	0.06	0.08	0.03	0.06
121	0.10	0.09	0.09	0.10	0.04	0.11
400	0.26	–	–	–	–	–
231	0.88	1.04	1.81	1.87	2.85	2.54
132	0.68	–	–	–	–	–
521	0.22	0.21	0.19	0.25	0.46	0.42
611	–	0.82	0.82	0.74	1.54	1.67
311	2.04	–	–	–	–	–

where $I(hkl)$ is the measured relative intensity, $I_0(hkl)$ stands for relative intensity given in JCPDS card for corresponding peak and n is the number of miller planes. The value of the texture coefficient cannot be greater than n and a value more than 1 represents the Preferred Orientation of planes in the sample. The values of TC for pristine and irradiated nanowires are tabulated in Table 2. The planes showing preferred orientation (i.e. T.C > 1) are shown in italic.

In case of the pristine sample, planes (001), (002) and (311) show the preferred orientation. On irradiation, (311) plane is completely removed and a new plane (611) appears. With the increase in fluence, TC of (001) plane decreases and that of planes (231) and (611) increases, which confirms that more and more planes orient in the direction of (231) and (611) after irradiation.

Variation of Texture Coefficient with Fluence for planes (001), (231) and (611) is as shown in Fig. 4. A change in the value of TC after the irradiation shows that irradiation has affected the orientation of crystallites, due to which some of the intensities have increased and some have decreased. We can also say that the intensity of some peaks was increased at the expense of other reflections. The energy imparted to the host material results in the plane orientation. The crystallinity and quality of the nanowires enhanced with the exposure to ions and increment in the peak intensity inferring that irradiation enlarges the crystallite size of the NWs. When a material is irradiated with ions, it may happen that the energy imparted to the material by energetic ion release the strain between grains which results in an additional increase in the crystal quality. The lattice vibration initiated by ionic particle helps the reorientation of these regions. Also, in this way intensity of a few planes will increase and of other planes decreases on irradiation.

Crystallite size was calculated from X-ray line broadening using Debye–Scherrer's formula; [30].

$$D = \frac{K\lambda}{\beta \cos\theta} \quad (3)$$

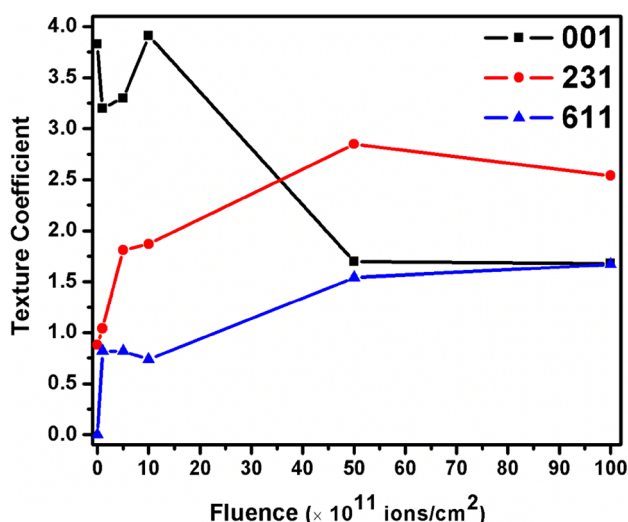


Fig. 4 Variation of texture coefficient with fluence for three major peaks

where D is average crystallite size, λ and β are X-ray wavelength and full width at half maxima respectively, θ is the Bragg's diffraction angle and k is the constant having value 0.94.

The density of dislocation (δ) and strain (ϵ) of the nanowires was calculated from XRD data using the following relations [31, 32].

$$\epsilon = \beta_s / 4 \tan \theta \quad (4)$$

$$\delta = 1/D^2 m^{-2} \quad (5)$$

where ϵ is the weighted average strain, β_s is for integral breadth of peak and θ is Bragg's angle and D is the average crystallite size.

Amorphization and grain fragmentation is a common process during exposure to energetic ions. Irradiation always leads to the breaking and formation of new grains. The average crystallite size for pristine case is found to be 23.20 nm which increases to a value of 28.77 nm for fluence 5×10^{12} ions/cm² but after that, a decrease in the crystallite size (21.7 nm) at last fluence was observed. Similarly, dislocation density and strain decreases up to a fluence 5×10^{12} ions/cm² and after that, an increase in their values was observed as evident from Table 3. An increase in crystallite size is a consequence of irradiation—induced grain growth.

3.3 Optical Studies

To explore the optical properties of pristine and irradiated nanowires, UV/Vis. Spectroscopic study was performed. Figure 5 gives optical absorption spectrum of pre and post-irradiated selenium nanowires. UV–visible spectra of the NWs have

Table 3 Average crystallite size, dislocation density and strain for pristine and irradiated samples

Fluence (ions/cm ²)	Average crystallite size (nm)	Dislocation density ($\times 10^{15}$)	Strain ($\times 10^{-3}$)
Pristine	23.2	1.86	1.1
1×10^{11}	23.6	1.79	1.0
5×10^{11}	26.3	1.45	0.99
1×10^{12}	28.3	1.25	0.92
5×10^{12}	28.8	1.21	0.88
1×10^{13}	21.7	2.13	1.2

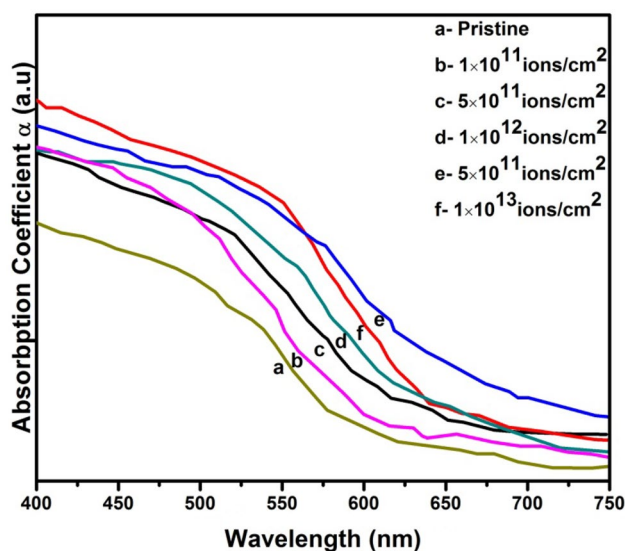


Fig. 5 Absorption plot of pristine and implanted selenium nanowires

recorded in the spectral range 400–750 nm after the removal of polycarbonate membrane. Absorption peak for pristine sample was observed at 585 nm and was shifted toward higher wavelength up to fluence 5×10^{12} ions/cm². An increment in the absorption with fluence indicates the production of defect states within the energy band gap or increased crystallization.

Estimation of the band gap of pristine and irradiated samples was done with the help of Tauc plot by plotting the $(\alpha h\nu)^2$ versus $(h\nu)$ and extrapolating the linear portion of absorption edge to the energy axis (X-axis) [33] as shown in Fig. 6a. Figure 6b shows the variation of band gap with ion fluence. α is the absorption coefficient and was measured using the relation $\alpha = A/t$, where A is the absorption and t is the thickness of the sample (10 μ m). The optical band gap (E_g) of all samples was analyzed with the help of following relation.

$$(\alpha h\nu) \propto (h\nu - E_g)^{1/2} \quad (6)$$

The optical band gaps for pristine and irradiated NWs for different fluence are given in Table 4.

Fig. 6 **a** Tauc plots of pristine and implanted selenium nanowires. **b** Variation of bang gap with fluence

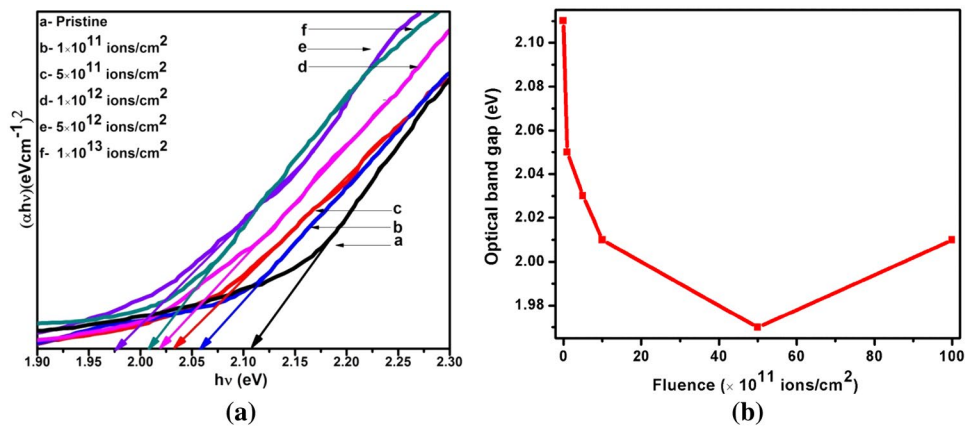


Table 4 Band gap for pristine and implanted nanowires

Ion fluence (ions/cm ²)	Band gap (eV)
Pristine	2.11
1×10^{11}	2.05
5×10^{11}	2.03
1×10^{12}	2.01
5×10^{12}	1.97
1×10^{13}	2.01

The band gap of the pristine nanowires was observed as 2.11 eV and decreased to a value of 1.97 eV till a fluence of 5×10^{12} ions/cm², after that increased to 2.01 eV at the last fluence. This increase or decrease in the band gap has been connected to the ion-induced grain growth or grain fragmentation [34, 35]. The defects created during irradiation create defect levels in the vicinity of the valence and conduction band edge resulting in the band tailing [36]. Along with this, an increase in the optical band gap at the last fluence can be related to the decrease in crystallite size (21.7 nm) at 1×10^{13} ions/cm².

3.4 Electrical Analysis

For realistic usage of semiconducting nanowires in device fabrication, the examination of their electrical properties becomes critical. Parameters like chemical composition, surface condition, diameter, crystal structure, and so on, of nanowires influence their electric behavior. Because of a large aspect ratio of nanowires, their surface energy increases which result in an increment of imperfections fixation and furthermore influences the conducting properties of nanowires. An arrangement of Ecopia Probe station along with two fine tungsten tip and Keithley 2400 source meter was utilized to record the current–voltage characteristic (IVC) of the nanowires (pristine and irradiated). Tungsten tip used for I–V measurement has a diameter of 10 μ m which

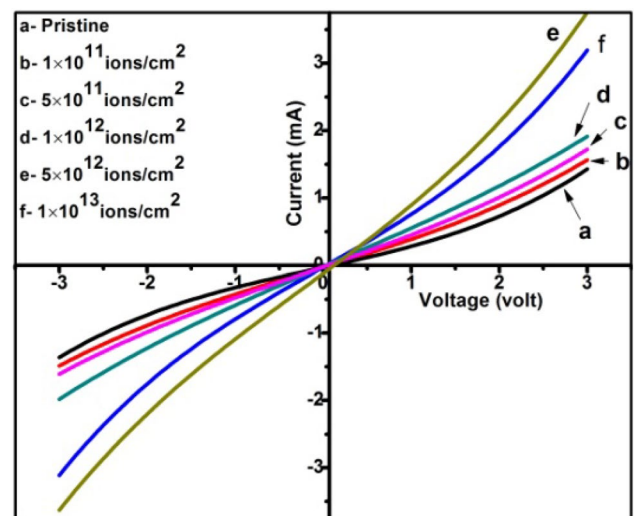


Fig. 7 I–V characteristic of pristine and irradiated selenium nanowires

covers around 480 nanowires and provides collective behavior of such amount of wires. Figure 7 displays the IVC of pre and post-irradiated nanowires in voltage range -3 V to 3 V.

The curves are nonlinear and are almost symmetric in positive and negative voltage region. To understand such type of behavior, in literature, many times Schottky or Tunnel barrier at the contacts are considered responsible. However, in the present case at low voltage, the curves are almost linear and do not show any rectifying nature.

As observed from Fig. 7 at low voltages, there is a linear relationship between current and voltage showing the ohmic character but with the increment in voltage, a transition from $I \propto V$ to $I \propto V^2$ behavior takes place which is a consequence of Space Charge Limiting Current (SCLC). Moreover, a linear graph between I/V versus V (Fig. 8) shows the quadratic dependence of current on voltage that is $I \propto V^2$. So, here we argue that the contacts are not totally of Schottky nature and some different factor is furthermore responsible for this

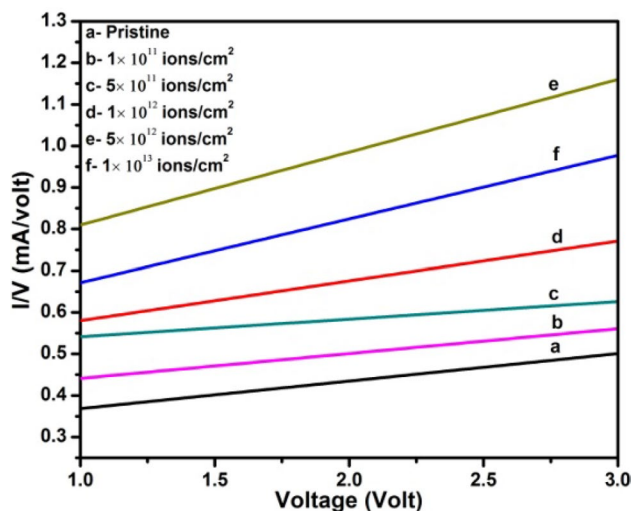


Fig. 8 Plots of current/voltage as a function of voltage for pristine and irradiated nanowires

type of behavior. This dependence of current on the square of the voltage is a clear sign of space charge limiting current (SCLC) and is an aftereffect of injection of a significant amount of electric charge from the contacts and a transition from ohmic behavior to SCLC or nonlinear behavior takes place.

The current density for such cases, as proposed by Talin et al. [37], is given by:

$$J = \zeta(R/L)\epsilon\mu \frac{V^2}{L^3} \quad (7)$$

where ϵ is the permittivity of the material, μ is the charge mobility, V is the applied voltage and L is the length of the NWs. $\zeta(R/L)$ is a scaling factor depending upon the aspect ratio and R is the radius of nanowires. When $R/L < 1$, SCLC in the specimen follow the expression:

$$J = \zeta(R/L)^{-2}\epsilon\mu \frac{V^2}{L^3}. \quad (8)$$

In the case of nanowires, SCLC has more dominance because of many reasons like poor electrostatic screening, carrier depletion and incorporation of charge traps during their synthesis [38–40]. From Fig. 6, it is clearly evident that with the fluence, the conductivity of the NWs increases up to a fluence of 5×10^{12} ions/cm² and after that, a decrease was observed in the conductivity. Generation of current carrier and creation of intermediate energy states in forbidden energy band is a common process during the passage of energetic ion which brings about the decrease in the forbidden energy band gap [41]. This generation of charge carriers and reduction in the barrier height result in the increase in conductivity of the NWs. It is confirmed

from the TRIM simulation that the energy imparted to the target material results in the ionization and atom displacement. Ionization process leads to an increase in the amount of free charge carriers consequently enhancing the conductivity. On the other hand, atom displacement gives rise to many defects in the material such as interstitial pairs, vacancies, point defects. The formation of defects is also supported by our observation of the reduction in the band gap of NWs, thus increasing the concentration of charge carriers. Apart from these, grain boundaries also play an important role in the conductivity of NWs. Grain boundaries act as a potential barrier for the charge carriers. Tunneling of carriers through grain boundaries depends upon this potential barrier. In any case, an increment in the crystallite size, as is clear from XRD analysis, brings about the reduction in grain boundaries because of which current carriers suffer a lesser amount of scattering contributing an increase in conductivity. Then again irradiation-induced defects and grain fragmentation rules at higher fluence (1×10^{13} particles/cm²) because of which a reduction in conductivity and crystallite size was observed [42, 43].

So, we can conclude that formation of intermediate states and generation of charge carriers dominates up to a fluence of 5×10^{12} ions/cm² resulting in an increase in the conductivity and after that, a decrease in the conductivity arise due to irradiation induced defects and grain fragmentation.

3.5 Impedance Analysis

Impedance spectra for different samples at room temperature were taken at 200 mV in the frequency range 20 Hz to 7 MHz. Impedance measurements consist of measuring the voltage and current with phase angle by applying sinusoidal voltage around a steady state value. A graph between Z' and frequency (Fig. 9) shows a variation of real impedance with frequency. A decrease in impedance for pristine nanowires was observed around 100 kHz and this decrease shifts towards higher frequency with fluence except for last two fluences. This reduction in the impedance might be because of the high capacitive coupling at higher frequency [44]. It was observed that the value of frequency shifts toward higher frequency at which impedance (Z') start decreasing for the first four fluences, which shows a decrease in the impedance.

But for last fluence, this value shifts toward the lower frequency, showing an increase in impedance. These results are in close agreement with I–V characteristics of the wires. In the frequency region below 10^5 Hz, Z' is independent of the frequency.

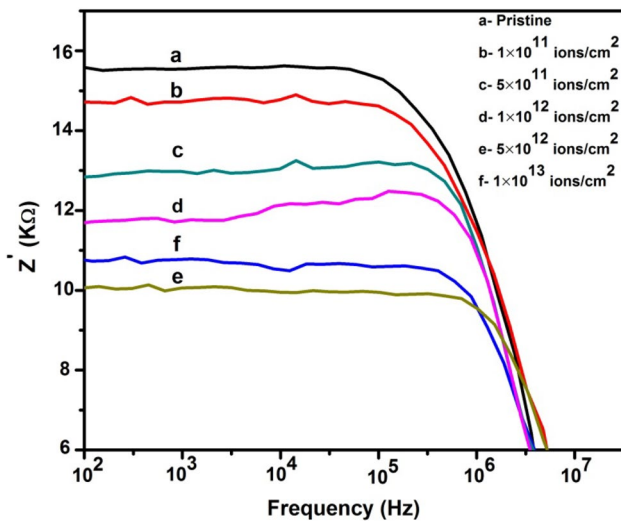


Fig. 9 Variation of a real part (Z') of impedance as a function of frequency for different fluence

4 Conclusion

The selenium nanowires of diameter 80 nm were irradiated with 80 MeV Ni^{6+} at different fluence ranging from 1×10^{11} to 1×10^{13} ions/cm². A variation in peak intensity was clearly observed without any other significant change in structural properties. A decrease in the optical band gap was also observed due to the creation of localized/intermediate states, which could be beneficial for their application in the opto-electronic field. An increase in the band gap seen at a higher fluence can be correlated to the induced grain fragmentation. SCLC model of transport is used to explain the electrical behavior. The electrical study demonstrates an increase in the conductivity at starting fluences (up to 5×10^{12} ions/cm²) that might be ascribed to the generation of charge carrier and increase in the crystallite size. A reduction in the conductivity at last fluence may be due to irradiation induced defects and grain fragmentation. A variation in the impedance with frequency was observed at different fluence, which may be due to the change in resistivity on irradiation of nanowires. Hence the choice of optimum fluence and energy irradiation with Ni^{6+} ions enhances the electric and optical properties of the Se NWs.


Acknowledgements Authors are thankful to IUAC, New Delhi, India, for providing material science beam line of 15UD pelletron for irradiation of the samples. We are also thankful for the assistance provided by the technical staff during irradiation experiment. A financial support provided by IUAC in the form of Project (IUAC/XIII.7/UFR-56303) also thankfully acknowledged.

References

1. Arnold, M.S., Avouris, P., Pan, Z.W., Wang, Z.L.: Field-effect transistors based on single semiconducting oxide nanobelts. *J. Phys. Chem. B* **107**, 659–663 (2003)
2. Martel, R., Schmidt, T., Shea, H.R., Hertel, T., Avouris, P.: Single- and multi-wall carbon nanotube field-effect transistors. *Appl. Phys. Lett.* **73**, 2447–2449 (1998)
3. Wang, Z.L.: Piezoelectric nanogenerators based on zinc oxide nanowire. *Arrays Sci.* **80**(312), 242–246 (2006)
4. Feng, X., Shankar, K., Varghese, O.K., Paulose, M., Latempa, T.J., Grimes, C.: Vertically aligned single crystal TiO_2 nanowire arrays grown directly on transparent conducting oxide coated glass: synthesis details and applications. *Nano Lett.* **8**, 3781–3786 (2008)
5. Gates, B., Mayers, B., Cattle, B., Xia, Y.: Synthesis and characterization of uniform nanowires of trigonal selenium. *Adv. Funct. Mater.* **12**, 219 (2002)
6. Shoaf, C.R., Heizer, W.D., Caplow, M.: Uptake of the components of phenylalanylphenylalanine and maltose by intestinal epithelium. *Biochim. Biophys. Acta Biomembr.* **600**, 939–949 (1980)
7. Liao, F., Han, X., Zhang, Y., Chen, H., Xu, C.: CTAB-assisted solvothermal synthesis of ultralong t-selenium nanowires and bundles using glucose as green reducing agent. *Mater. Lett.* **214**, 41–44 (2018)
8. Kumar, N., Kumar, R., Kumar, S., Chakarvarti, S.K.: Microstructural, optical and electrical investigations of large scale selenium nanowires prepared by template electrodeposition. *J. Mater. Sci. Mater. Electron.* **25**, 3537–3542 (2014)
9. Steichen, M., Dale, P.: Synthesis of trigonal selenium nanorods by electrodeposition from an ionic liquid at high temperature. *Electrochem. Commun.* **13**, 865–868 (2011)
10. Chen, H., Shin, D.W., Nam, J.G., Kwon, K.W., Yoo, J.B.: Selenium nanowires and nanotubes synthesized via a facile template-free solution method. *Mater. Res. Bull.* **45**, 699–704 (2010)
11. Huczko, A.: Template-based synthesis of nanomaterials. *Appl. Phys. A* **70**(4), 365–376 (2000)
12. Jain, I.P., Agarwal, G.: Ion beam induced surface and interface engineering. *Surf. Sci. Rep.* **66**, 77–172 (2011)
13. Avasthi, D.: Modification and characterisation of materials by swift heavy ions. *Def. Sci. J.* **59**, 401–412 (2009)
14. Kanjilal, D.: Swift heavy ion-induced modification and track formation in materials. *Curr. Sci.* **80**, 1560–1566 (2001)
15. Kumar, V., Jaiswal, M.K., Gupta, R., Ram, J., Sulania, I., Ojha, S., et al.: Effect of low energy (keV) ion irradiation on structural, optical and morphological properties of SnO_2 - TiO_2 nanocomposite thin films. *J. Mater. Sci. Mater. Electron.* **29**(15), 13328–13336 (2018)
16. Chauhan, V., Gupta, T., Koratkar, N., Kumar, R.: Studies of the electronic excitation modifications induced by SHI of Au ions in RF sputtered ZrO_2 thin films. *Mater. Sci. Semicond. Process.* **88**, 262–272 (2018)
17. Kumar, R., De, U., Prasad, R.: Physical and chemical response of 70 MeV carbon ion irradiated polyether sulphone polymer. *Nucl. Instrum. Methods Phys. Res. Sect. B Beam Interact. Mater. Atoms* **248**(2), 279–283 (2006)
18. McPherson, M.: Infrared photoconduction in radiation-damaged silicon diodes. *J. Opt. A Pure Appl. Opt.* **7**, S325–S330 (2005)
19. Pillai, V.R.V., Khamari, S.K., Dixit, V.K., Ganguli, T., Kher, S., Oak, S.M.: Effect of γ -ray irradiation on breakdown voltage, ideality factor, dark current and series resistance of GaAs p–i–n diode. *Nucl. Instrum. Methods Phys. Res. Sect. A Accel. Spectrom. Detect. Assoc. Equip* **685**, 41–45 (2012)
20. Choudhary, R., Chauhan, R.P.: Swift heavy ion induced modifications in optical and electrical properties of cadmium selenide thin films. *Electron. Mater. Lett.* **13**(4), 330–338 (2017)

21. Mishra, M., Alwarappan, S., Kanjilal, D., Mohanty, T.: The effect of low energy nitrogen ion implantation on graphene nanosheets. *Electron. Mater. Lett.* **14**(4), 488–498 (2018)
22. Panchal, S., Chauhan, R.P.: Lithium ion beam impact on selenium nanowires. *Phys. E Low Dimens. Syst. Nanostruct.* **87**, 37–43 (2017)
23. Panchal, S., Chauhan, R.P.: Krypton ion implantation effect on selenium nanowires. *Phys. Lett. A* **381**, 2636–2642 (2017)
24. Gehlawat, D., Chauhan, R.P.: Swift heavy ions induced variation in the electronic transport through Cu nanowires. *Mater. Chem. Phys.* **145**, 60–67 (2014)
25. Narula, C., Chauhan, R.P.: High dose gamma ray exposure effect on the properties of CdSe nanowires. *Radiat. Phys. Chem.* **144**, 405–412 (2018)
26. Paroni, R.: Optimal bounds on texture coefficients. *J. Elast. Phys. Sci. Solids* **60**(1), 19–34 (2000)
27. Cullity, B.D.: *Elements of X-ray Diffraction*, 2nd edn. Addison-Wesley Publishing Company Inc, Reading (1978)
28. Barrett, C.S., Massalski, T.B.: *Structure of metals: crystallographic methods, principles and data*. In: *International Series on Materials Science and Technology*, vol. 35, 3rd edn, pp. 1–654. Pergamon (1980)
29. Harris, G.B.: Quantitative measurement of preferred orientation in rolled uranium bars. *Philos. Mag. J. Sci.* **43**, 113–123 (1952)
30. Cullity, B.D., Stock, S.R.: *Elements of X-ray Diffraction*, 3rd edn Prentice Hall, New York, pp. 174–177 (2001)
31. Stokes, A.R., Wilson, A.J.C.: The diffraction of X rays by distorted crystal aggregates—I. *Proc. Phys. Soc.* **56**, 174–181 (1944)
32. Williamson, G., Hall, W.: X-ray line broadening from filed aluminium and wolfram. *Acta Metall.* **1**, 22–31 (1953)
33. Tauc, J., Menth, A.: States in the gap. *J. Non Cryst. Solids* **8–10**, 569–585 (1972)
34. Mohanta, D., Nath, S.S., Mishra, N.C., Choudhury, A.: Irradiation induced grain growth and surface emission enhancement of chemically tailored ZnS: Mn/PVOH nanoparticles by Cl^{+9} ion impact. *Bull. Mater. Sci.* **26**, 289–294 (2003)
35. Thakurdesai, M., Mahadkar, A., Kulriya, P.K., Kanjilal, D., Bhattacharyya, V.: Synthesis of nanodimensional TiO_2 thin films using energetic ion beam. *Nucl. Instrum. Methods Phys. Res. Sect. B Beam Interact. Mater. Atoms.* **266**, 1343–1348 (2008)
36. Townsend, P.D., Chandler, P.J., Zhang, L.: *Optical Effects of Ion Implantation*, vol. 13. Cambridge University Press, Cambridge (2006)
37. Talin, A.A., Léonard, F., Swartzentruber, B.S., Wang, X., Hersee, S.D.: Unusually strong space-charge-limited current in thin wires. *Phys. Rev. Lett.* **101**(7), 76802 (2008)
38. Léonard, F., Tersoff, J.: Novel length scales in nanotube devices. *Phys. Rev. Lett.* **83**, 5174–5177 (1999)
39. Gu, Y., Lauhon, L.J.: Space-charge-limited current in nanowires depleted by oxygen adsorption. *Appl. Phys. Lett.* **89**, 143102 (2006)
40. Schricker, A.D., Davidson, F.M., Wiacek, R.J., Korgel, B.A.: Space charge limited currents and trap concentrations in GaAs nanowires. *Nanotechnology* **17**, 2681–2688 (2006)
41. Kannappan, P., Asokan, K., Krishna, J.B.M., Dhanasekaran, R.: Effect of SHI irradiation on structural, surface morphological and optical studies of CVT grown ZnSSe single crystals. *J. Alloys Compd.* **580**, 284–289 (2013)
42. Kumar, N., Kumar, R., Kumar, S., Chakarvarti, S.K.: Modifications in optical and electrical properties of selenium nanowire arrays using ion beam irradiation. *Appl. Phys. A* **121**, 571–579 (2015)
43. Rani, S., Puri, N.K., Roy, S.C., Bhatnagar, M.C., Kanjilal, D.: Effect of swift heavy ion irradiation on structure, optical, and gas sensing properties of SnO_2 thin films. *Nucl. Instrum. Methods Phys. Res. Sect. B Beam Interact. Mater. Atoms* **266**, 1987–1992 (2008)
44. Veit, W., Diestel, H., Pregla, R.: Coupling of crossed planar multiconductor systems *IEEE. Trans. Microw. Theory Tech.* **38**, 265–269 (1990)

Affiliations

Suresh Panchal¹ · R. P. Chauhan¹ 

✉ R. P. Chauhan
chauhanrpc@gmail.com; sony.spanchal@gmail.com

¹ Department of Physics, National Institute of Technology, Kurukshetra, Haryana 136119, India